Current Optics and Photonics
Vol. 3, No. 1, February 2019, pp. 40-45

ISSN: 2508-7266(Print) / ISSN: 2508-7274(Online)
DOI: https://doi.org/10.3807/COPP.2019.3.1.040

Tuning Photoluminescence of Biological Light Emitters via Silk Protein Based Resonators

Sara Arif[1], Muhammad Umar[1], and Sunghwan Kim[1,2]*

[1]*Department of Energy Systems Research, Ajou University, Suwon 16499, Korea*
[2]*Department of Physics, Ajou University, Suwon 16499, Korea*

(Received November 20, 2018 : revised December 16, 2018 : accepted December 19, 2018)

Adding tunability to biological light emitters offers an unprecedented technique in biological sensing and imaging. Here, we report a tunable, lithographic-free, planar, and ultrathin metal-insulator-metal (MIM) resonator capable of tuning the optical properties solely by a silk/sodium fluorescein hydrogel layer, a biocompatible light emitter. In water, the volume of the resonator was expanded by swelling, and then the resonant mode could be shifted. Simulations predicted the red-shifted resonance peak in transmission when the MIM was swollen in water. The red-shift could be attributed to the increase in the thickness of the silk hydrogel layer due to the absorbed water. The shift of the resonance could affect the fluorescence of the dye in the silk hydrogel layer.

Keywords : Silk protein, Tunable luminescence, Metal-insulator-metal resonator, Hydrogel
OCIS codes : (160.1435) Biomaterials; (230.5750) Resonators

I. INTRODUCTION

Photoluminescence (PL) tuning is an important subject due to its significant applications in lasers, telecommunications, biomarkers, and medical imaging [1, 2]. PL spectra have been used to study the characteristic features, even impurities of fluorescent substances via several light-emitting meta-structures [3]. Tuning of the photoluminescence has been achieved through the alteration of aggregated structures within various devices such as quantum dot light-emitting devices [3], metamaterials with Fano resonance [4] and piezoelectric single-crystals [5]. These devices no doubt, are operative for fluorescence tuning, but the involved experimental progressions are complex and the non-economical fabrication techniques limit the applications.

To overcome all these problems, ultra-thin multilayered planar resonators are a better choice especially due to the delicate control over the spectral properties and the manipulation of light-matter interactions. The flexibility of the spectral engineering and design of these planar and multilayered optical structures give the advantages of cost-effective fabrication, high sensitivity, selectivity and availability [6-10]. Moreover, the exciting optical functions such as optical resonances [11], field localization [12], refractive index (RI) engineering [13], phase and amplitude control [14], etc., are achieved simply by modifying the size, shape and dielectric material of these planar devices [15-18]. For instance, highly efficient spectral properties of the planar metal-insulator-metal (MIM) resonators, based on the Fabry-Perot etalon principle, have been used to tune the PL spectrum.

Here, we report a planar ultrathin tunable transmission color filter based on metal-insulator-metal (MIM) resonators capable of tuning the optical properties solely by the film thickness and RI of the insulating material. Silk fibroin, the natural protein extracted from the *Bombyx Mori*, has emerged as an excellent dielectric material in optics and light manipulating fields due to its optical transparency and unique mechanical behavior [19-21]. It has been used in various devices such as photonic crystals [22, 23], waveguides [24, 25], and single-mode lasers [26, 27]. The hydrogel form of silk is capable of inducing drastic changes in the optical resonances due to its ability to swell and shrink [28]. These properties of silk in MIM resonators can tune the spectral outcome. The intermediate silk hydrogel layer serving as a dielectric between two metal layers is

*Corresponding author: sunghwankim@ajou.ac.kr, ORCID 0000-0002-6097-5630
Color versions of one or more of the figures in this paper are available online.

This is an Open Access article distributed under the terms of the Creative Commons Attribution Non-Commercial License (http://creativecommons.org/licenses/by-nc/4.0/) which permits unrestricted non-commercial use, distribution, and reproduction in any medium, provided the original work is properly cited.

Copyright © 2019 Current Optics and Photonics

mixed with sodium fluorescein. The optical pumping can excite the electrons of sodium fluorescein in the film sandwiched between two metal films and upon de-excitation, it emits photons which exhibit a PL spectrum. The objective of this study was to fine-tune the PL spectrum of sodium fluorescein by altering the thickness and refractive index of silk in an MIM resonator. This is achieved by simply water absorbance.

II. METHODS

Preparation of silk aqueous solution: The cocoons of *Bombyx mori* caterpillars were boiled in a 0.02 M NaCl solution. The fibroin was rinsed with distilled water and air dried for 24 h. The dried fibroin was dissolved in a 9.3 M LiBr solution for 4 h at 60°C, yielding a 20 wt% aqueous solution. This solution was dialyzed to 6% in the cellulose tubular membrane for 2 days at room temperature followed by centrifugation and syringe filtration with a 0.45 μm pore size.

Fabrication process: The bottom silver layer 30 nm thick was deposited on the square quartz substrates of 2×2 cm^2 using an electron beam evaporating process. An 8 wt% of sodium fluorescein salt solution was mixed in 6 wt% silk aqueous solution. This solution was coated on the silver layer by using a spin-coater up to 130 nm thickness. The thickness of the blended silk spacer could be controlled by the concentration of silk and by the revolution of the spin coater which was set to 5.77% and 3900 rpm. To convert silk/sodium fluorescein solution into the hydrogel, the sample was dipped into methanol for 1 min and air dried. Then the top layer of silver of 30 nm was deposited on the silk/sodium fluorescein hydrogel by the same electron beam evaporation method.

Simulation: To perform the numerical simulations, we used a commercially available finite-difference time domain (FDTD) software package (FDTD, Lumerical Solutions). Simulations were carried out in the 2D layout. The 300 nm unit cell was selected along the *x*-axis and the boundary conditions were imposed on the lateral directions. The plane wave source was placed inside the MIM device along the +y direction and for comparison purpose it was moved outside of the device. The wavelength range for this plane source was 300~1000 nm with 2000 frequency points. The transmission was recorded by means of the power monitor below the silver layer. The 2D field profile monitors in *x-y* plane showed the electric and magnetic field distribution across the cross-section of the MIM. The complex refractive index of Ag and silk and quartz was taken from the data of Palik [29].

Optical measurement: For transmission measurements, optic fibers with a 400 μm core diameter were used, one for directing and the other one for collecting the light from the sample. The white light source was placed in the vertical direction, while the transmitted signal was displayed by using an optical spectrum analyzer via an optic fiber. The MIM samples were pumped by the continuous wave from the Nd: YAG laser. The diameter 0.25 μm incident beam was focused on the sample with the help of lenses. The resulting signals were collected by optic fiber and directed to an optical spectrum analyzer.

III. RESULTS

The MIM device was fabricated with e-beam silver deposition and followed by spin coating of the silk layer Fig. 1(a). Silk protein mixed with sodium fluorescein was sandwiched between top and bottom ultrathin Ag layers (30 nm each) and this insulating layer was treated with methanol to induce β-sheet crystallization through the formation of hydrogen bonds between silk molecules, which transforms the soluble silk solution into the hydrogel [9, 10, 30]. This MIM resonator mimics the Fabry-Perot etalon principle that depends upon the variations of thickness and refractive index of the insulating layer resulting in different resonance peaks Fig. 1(b).

FDTD simulations were carried out by assuming a light source (in the range of 400~1000 nm wavelength) first positioned inside the dielectric (silk/sodium fluorescein) of the MIM and then moved outside of the MIM resonator for the comparison. These simulations were studied in the presence of air and water medium sequentially (Fig. 2(a)). The resonance peak is red-shifted due to the swelling of silk in the water medium irrespective of the light source position. In the air medium, the wavelength is shorter and is possibly due to the dry state of silk hydrogel as compared to for the water medium. Again, the position of the light source makes no difference, while the thickness of the dielectric material is the determining factor in the output transmission spectra. The FDTD simulation also predicted the change in the thickness of the silk/sodium fluorescein layer from 115 nm in the air medium to 190 nm as a result of water absorbance. To validate these simulation results, the experimental setup with the light source placed outside was established to record the transmission spectra of the silk/sodium fluorescein layer in the MIM device. In the air medium, the dry state of the silk/sodium fluorescein layer transmits a resonance peak of wavelength ~530 nm while in the water medium, the red-shifted wavelength ~695 nm was observed, as shown in Fig. 2(b). These experimental results are in strong agreement with those of simulation predictions when the source is placed outside. However, for the placement of the light source inside the MIM cavity, the experimental setup is not viable due to the nano-dimensions of the MIM resonator. Therefore, to further investigate the effect of inside light source positioning, more FDTD simulations were performed varying the transmitted electric field (TE) and the magnetic field (TM) intensities.

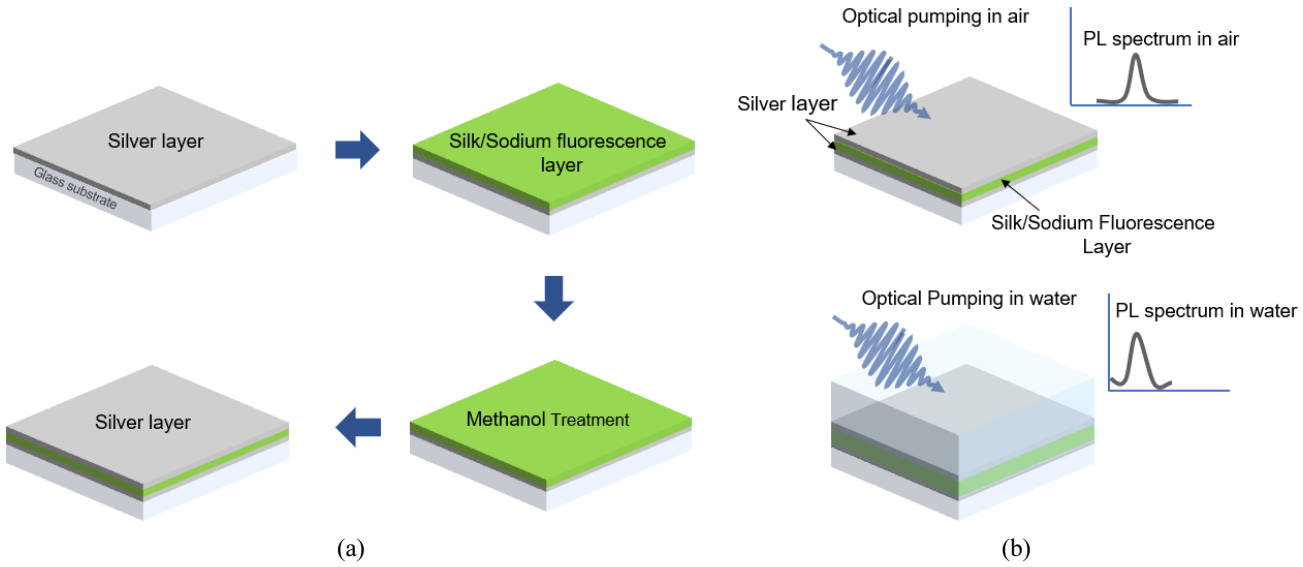

FIG. 1. (a) The fabrication process of the MIM resonator. (b) The schematic working principle of the MIM device. The measured spectra of silk mixed with sodium fluorescein MIM in the dry and wet state are shown. Note that the silk in the expanded state can tune the transmission spectra.

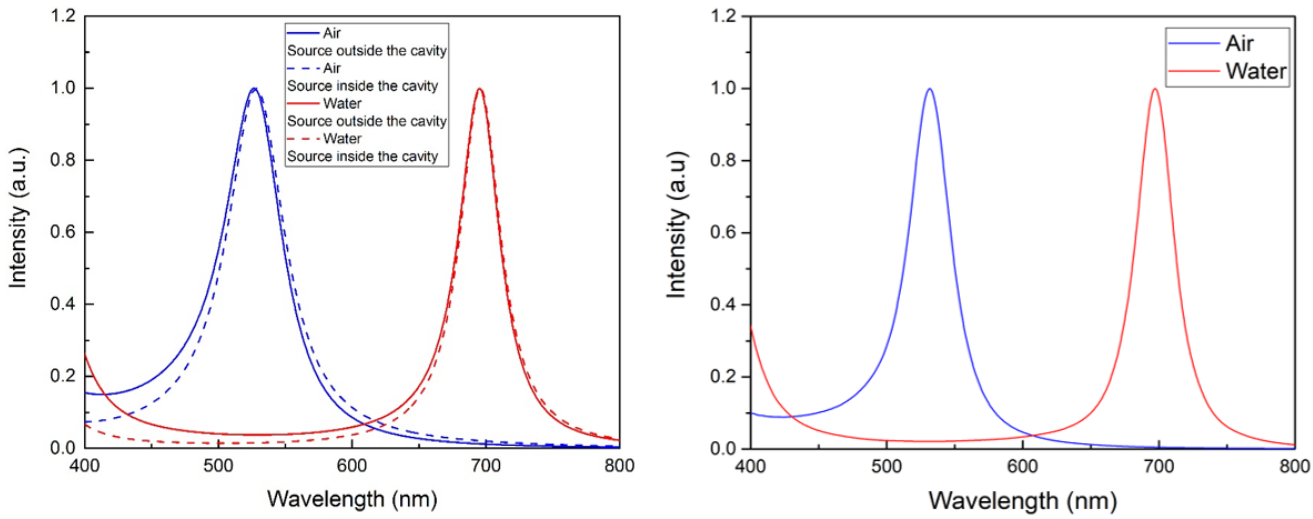

FIG. 2. (a) FDTD simulation results for transmission with the source inside and outside. (b) Experiment results for transmission peaks in the air and wet state with a source outside of MIM.

The stimulated TE and TM intensities transmitted through air and water media in relation to the light source position inside and outside of the three-layer MIM cavity are shown in Fig. 3. In both media, the electric field is highly confined at the dielectric section between two metallic films, where a standing wave is formed due to constructive interference of incoming and reflected waves. In air and water media, transmitted wavelengths of ~526 nm and 695 nm were recorded, respectively, regardless of the light source position. In short, the effect of the medium is the red-shift, which is a result of the increase in the thickness of the MIM hydrogel cavity.

To study the photoluminescence of the sodium fluorescein, optical pumping was done with the Nd: YAG laser of $\lambda = 355$ nm as shown in Fig. 4(a). The incidence angle of the laser beam on the resonator was fixed at 0°, and the diameter of the laser spot on the film was 0.25 μm. The sodium fluorescein absorbs the incoming radiation from the pumping source which excites the electrons from ground state to excited state then the excited electron emits the photon and jumps back to the initial state. The emitted photons exhibit the PL spectrum. The PL spectrum in the expanded state of silk is blue-shifted by ~22 nm as the resonance peaks in air and water are at ~537 nm and

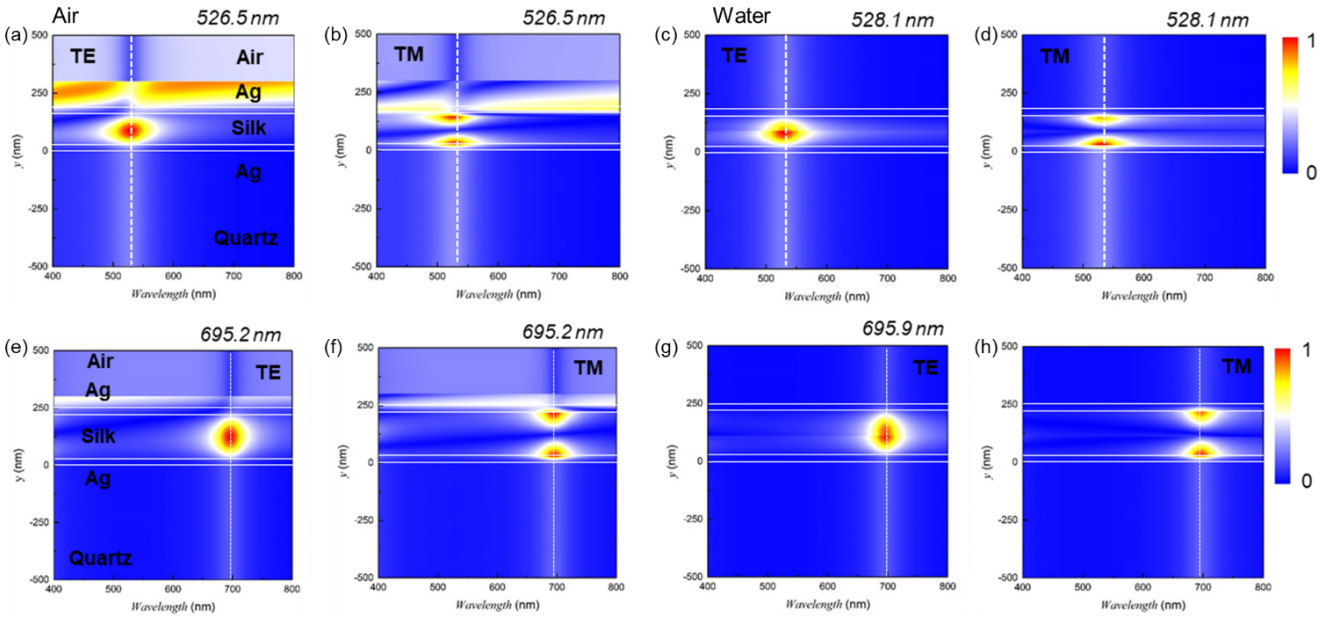

FIG. 3. Electric (TE) and magnetic field (TM) confinement at corresponding transmission wavelength when the source is outside in air (a,b), and in water (c,d). When the source is outside the cavity, in air (e,f) and in water medium (g,h).

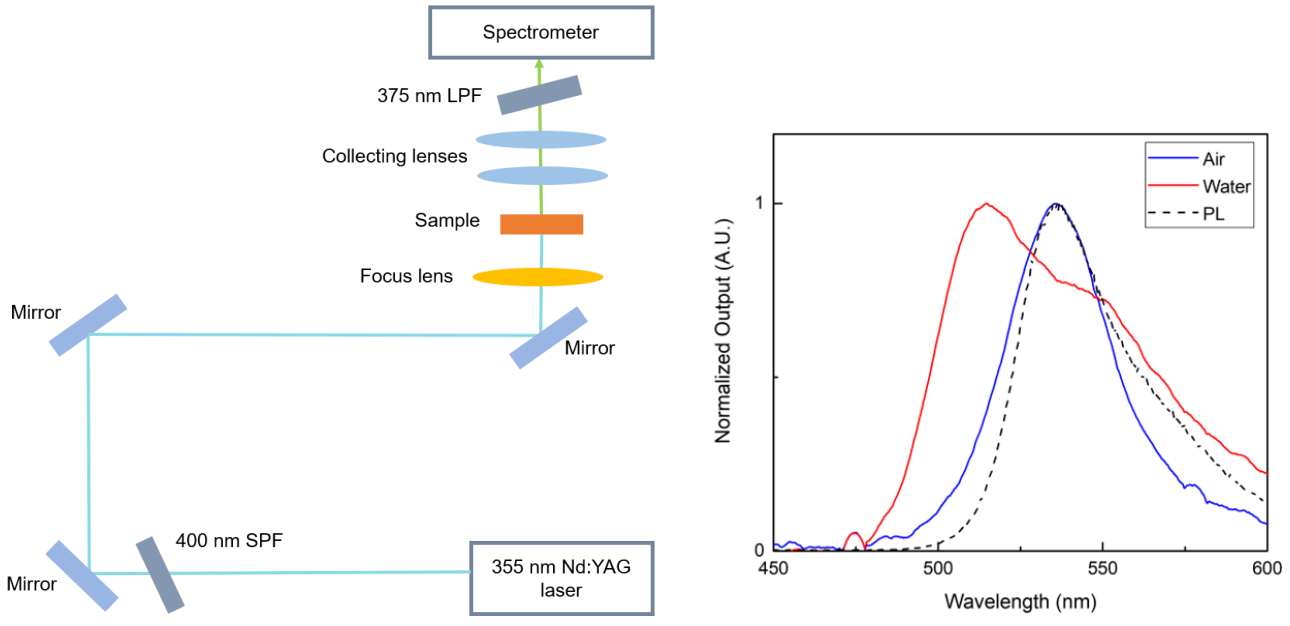

FIG. 4. (a) Vertical laser setup for optical pumping. (b) Display of PL spectrum of Sodium Fluorescein in air and water media.

~515 nm respectively (Fig. 4(b)). The fluorescent molecule emits light in random directions. It bounces back and forth between two metal layers and exhibits constructive interference at some specified angle. This angle is a crucial factor in tuning the PL spectrum and results in a blue-shift in the water medium when the thickness of the MIM cavity has increased.

IV. DISCUSSION

Since the MIM cavity follows Fabry-Perot-like behavior, only the small proportion of the incident light wavelength is trapped and transmitted which is selected via the resonance wavelength of the MIM cavity. This determining resonance wavelength of the MIM cavity follows the following equation.

$$2\left(\frac{2\pi}{\lambda}\right)ndcos\theta+\phi_a+\phi_b=2\pi m \quad (1)$$

where λ, n, θ and d correspond to the resonance wavelength, the refractive index, the incidence angle, and the thickness of the MIM dielectric, respectively. The terms φ_a and φ_b show the phase shift due to reflection from the bottom and the top metal layers, respectively. The order of the MIM cavity mode is an integer m. For the light to be trapped inside the MIM cavity, the phase condition (2 πm) in Eq. (1) must be satisfied, which means to enable the constructive interference in each full round trip, the left-hand side of the equation should be an integer multiple of 2π. Finally, constructive interference makes the enhanced transmission of light through the cavity possible [31, 32].

$$\left(\frac{4\pi}{\lambda}\right)ndcos\theta+2\phi=2\,\pi m \quad (2)$$

From Eq. (2), the wavelength of the peak transmission is

$$\lambda=\frac{2\pi ndcos\theta}{\pi m-\phi} \quad (3)$$

From Eq. (3) the position of the peak transmission depends on the angle of incidence such that maximum λ occurs when $\theta=0$ for a specified thickness and refractive index of the medium. Increasing the medium thickness for a particular value of θ, the peak transmission yields a red-shift. The peak transmission shows blue shift with increasing the incident angle θ for a specified thickness. For tuning the resonance behaviors, the volume change of the dielectric layers is crucial. The tuning of the PL spectrum depends upon the incident angle inside the cavity, RI and the width of the cavity. When the MIM resonator is immersed in water, the silk absorbs the water molecules thus increases the thickness of the dielectric which changes the position of the fluorescein molecules. As the fluorescein molecule emits light in random directions and the change in position of molecules induces the electric field between the silver layers at some specified angle, and hence shows the blue-shift in resonance wavelength of the PL spectrum. For some specified θ, increase in thickness d ~80 nm and decrease in refractive index of silk from $n_{silk}=1.54$ to $n_{silk\text{-}swelled}=1.43$, Eq. (3) yields the shorter wavelength. The tuning of the PL spectra also depends upon the incident angle along with the thickness and RI of the spacer.

V. CONCLUSION

Our experimental results and theoretical explanation indicate that the dimension of the MIM cavity and the incident angle of light enable the tuning effect of the PL spectrum. In this study, post casting of the silk mixed with sodium fluorescein serving as an intermediate layer for film formation on the fabricated MIM resonator yielded a tunable MIM resonator. The FDTD simulations for the light source placed inside and outside in the dielectric silk/sodium fluorescein (cavity) of the MIM resonator, for both air and water media, were performed. Irrespective of the light source position, the simulation results predicted the red-shifted resonance peak in a water medium, which was a consequence of the increase in thickness of the silk layer. For transmission spectra, experimental results match well with those of simulation. The PL spectrum was tuned in the water medium due to the increase in the thickness of silk hydrogel and the angular dependence of the emitted light from the sodium fluorescein between the insulating layers.

ACKNOWLEDGEMENT

The authors acknowledge support from the GRRC program of Gyeonggi province (GRRC-AJOU-2016-B01, Photonics-Medical Convergence Technology Research Center, and the Korea Institute of Energy Technology Evaluation and Planning (no. 20164030201380, Human Resources Program in Energy Technology).

REFERENCES

1. R. V. Deun, P. Nockemann, C. G. Walrand, and K. Binnemans, "Strong erbium luminescence in the near-infrared telecommunication window," Chem. Phys. Lett. **397**, 447-450 (2004).
2. T. Otto, S. Kurth, S. Voigt, A. Morschhauser, M. Meinig, K. Hiller, M. Moebius, and M. Vogel1, "Integrated microsystems for smart applications," Sens. Mater. **30**, 767-778 (2018).
3. X. Jin, L. Dong, X. Di, H. Huang, J. Liu, X. Sun, X. Zhang, and H. Zhu, "NIR luminescece for the detection of latent fingerprints based on ESIPT and AIE processes" RSC Adv. **5**, 87306-87310 (2015).
4. Y. Moritake, Y. Kanamori, and K. Hane, "Emission wavelength tuning of fluorescence by fine structural control of optical metamaterials with fano resonance," Sci. Rep. **6**, 33208 (2016).
5. F. Wang, D. Liu, Z. Chen, Z. Duan, Y. Zhang, D. Sun, X. Zhao, W. Shi, R. Zheng, and H. Luo, "*In situ* reversible tuning of photoluminescence of an epitaxial thin film via piezoelectric strain induced by a $Pb(Mg_{1/3}Nb_{2/3})O_3$-$PbTiO_3$ single crystal," J. Mater. Chem. C **5**, 9115-9120 (2017).
6. E. Rajo-Iglesias, O. Quevedo-Teruel, and L. Inclan-Sanchez, "Mutual coupling reduction in patch antenna arrays by using a planar EBG structure and a multilayer dielectric substrate," IEEE Trans. Antennas Propag. **56**, 1648-1655 (2008).
7. G. T. Papadakis, D. Fleischman, A. Davoyan, P. Yeh, and H. A. Atwater, "Optical magnetism in planar metamaterial heterostructures," Nat. Commun. **9**, 296 (2018).
8. H. Wohltjen and A. W. Snow, "Colloidal metal-Insulator-

metal ensemble chemiresistor sensor," Anal. Chem. **70**, 2856-2859 (1998).
9. H. Kwon and S. Kim, "Chemically tunable, biocompatible, and cost-effective metal-insulator-metal resonators using silk protein and ultrathin silver films," ACS Photon. **2**, 1675-1680 (2015).
10. M. Umar, K. Min, M. Jo, and S. Kim, "Ultra-thin, conformal, and hydratable color-absorbers using silk protein hydrogel," Opt. Mater. **80**, 241-246 (2018).
11. D. M. Zhigunov, A. B. Evlyukhin, A. S. Shalin, U. Zywietz, and B. N. Chichkov, "Femtosecond laser printing of single Ge and SiGe nanoparticles with electric and magnetic optical resonances," ACS Photon. **5**, 977-983 (2018).
12. A. D. Mayevsky and A. M. Funston, "Control of electric field localization by three-dimensional bowtie nanoantennae," Phys. Chem. C **122**, 18012-18020 (2018).
13. S. Novak, P. T. Lin, C. Li, C. Lumdee, J. Hu, A. Agarwal, P. G. Kik, W. Deng, and K. Richardson, "Direct electrospray printing of gradient refractive index chalcogenide glass films," ACS Appl. Mater. Inter. **9**, 26990-26995 (2017).
14. E. Mårsell, E. Boström, A. Harth, A. Losquin, C. Guo, Y.-C. Cheng, E. Lorek, S. Lehmann, G. Nylund, M. Stankovski, C. L. Arnold, M. Miranda, K. A. Dick, J. Mauritsson, C. Verdozzi, A. L'Huillier, and A. Mikkelsen, "Spatial control of multiphoton electron excitations in InAs nanowires by varying crystal phase and light polarization," Nano Lett. **18**, 907-915 (2018).
15. Z. Li, S. Butun, and K. Aydin, "Large-area, lithography-free super absorbers and color filters at visible frequencies using ultrathin metallic films," ACS Photon. **2**, 183-188 (2015).
16. K. T. Lee, S. Seo, and L. J. Guo, "High-color-purity subtractive color filters with a wide viewing angle based on plasmonic perfect absorbers," Adv. Opt. Mater. **3**, 347-352 (2015).
17. M. Yan, "Metal-insulator-metal light absorber: a continuous structure," J. Opt. **15**, 025006 (2013).
18. H. Shin, M. F. Yanik, S. Fan, R. Zia, and M. L. Brongersma, "Omnidirectional resonance in a metal-dielectric-metal geometry," Appl. Phys. Lett. **84**, 4421-423 (2004).
19. F. G. Omenetto and D. L. Kaplan, "A new route for silk," Nat. Photon. **2**, 641-643 (2008).
20. F. G. Omenetto and D. L. Kaplan, "New opportunities for an ancient material," Science **329**, 528-531 (2010).
21. K. Min, M. Umar, S. Roy, S. Lee, and S. Kim, "Silk protein as a new optically transparent adhesive layer for an ultra-smooth sub-10 nm gold layer," Nanotechnology **28**, 115201 (2017).
22. S. Kim, A. N. Mitropoupls, J. D. Spitzberg, H. Tao, D. L. Kaplan, and F. G. Omenetto, "Silk inverse opals," Nat. Photon. **6**, 818-823 (2012).
23. K. Min, S. Kim, and S. Kim, "Deformable and conformal silk hydrogel inverse opal," Proc. Natl. Acad. Sci. **114**, 6185 (2017).
24. S. T. Parker, P. Domachuk, J. Amsden, J. Bressner, J. A. Lewis, D. L. Kaplan, and F. G. Omenetto, "Biocompatible silk printed optical waveguides," Adv. Mater. **21**, 2411-2415 (2009).
25. V. Prajzler, K. Min, S. Kim, and P. Nekvindova, "The investigation of the waveguiding properties of silk fibroin from the visible to near-infrared spectrum," Materials **11**, 112 (2018).
26. H. Jung, K. Min, H. Jeon, and S. Kim, "Physically transient distributed feedback laser using optically activated silk bio-ink," Adv. Opt. Mater. **4**, 1738-1743 (2016).
27. Y. Choi, H. Jeon, and S. Kim, "A fully biocompatible single-mode distributed feedback laser," Lab Chip **15**, 642-645 (2015).
28. M. Lee, H. Jeon, and S. Kim, "A highly tunable and fully biocompatible silk nanoplasmonic optical sensor," Nano Lett. **15**, 3358-3363 (2015).
29. E. Palik, *Handbook of Optical Constants of Solids: Index* (Elsevier, New York, 1998), Vol. 3.
30. X. Hu, D. Kaplan, and P. Cebe, "Determining beta-sheet crystallinity in fibrous proteins by thermal analysis and infrared spectroscopy," Macromolecules **39**, 6161-6170 (2006).
31. J. Stone and L. Stulz, "Pigtailed high-finesse tunable fibre Fabry-Perot interferometers with large, medium and small free spectral ranges," Electron. Lett. **23**, 781-783 (1987).
32. A. Frenkel and C. Lin, "Angle-tuned etalon filters for optical channel selection in high density wavelength division multiplexed systems," J. Lightw. Technol. **7**, 615-624 (1989).